PCCP

The Role of High-Density and Low-Density Amorphous Ice on Biomolecules at Cryogenic Temperatures: A Case Study with Polyalanine

Journal:	*Physical Chemistry Chemical Physics*
Manuscript ID	CP-ART-06-2021-002734.R1
Article Type:	Paper
Date Submitted by the Author:	16-Aug-2021
Complete List of Authors:	Eltareb, Ali; Brooklyn College, Physics; CUNY The Graduate Center, Lopez, Gustavo; Lehman College of the City University of New York, Chemistry Giovambattista, Nicolas; CUNY, Brooklyn College

The Role of High-Density and Low-Density Amorphous Ice on Biomolecules at Cryogenic Temperatures: A Case Study with Polyalanine

Ali Eltareb[1,2,*], Gustavo E. Lopez[3,4,*], and Nicolas Giovambattista[1,2,4*]

[1] *Department of Physics, Brooklyn College of the City University of New York, Brooklyn, New York 11210, United States*

[2] *Ph.D. Program in Physics, The Graduate Center of the City University of New York, New York, NY 10016*

[3] *Department of Chemistry, Lehman College of the City University of New York, Bronx, New York 10468, United States*

[4] *Ph.D. Program in Chemistry, The Graduate Center of the City University of New York, New York, NY 10016*

E-mail: ali.eltareb@brooklyn.cuny.edu,gustavo.lopez1@lehman.cuny.edu,ngiovambattista@brooklyn.cuny.edu

Abstract

Experimental techniques, such as cryo-electron microscopy, require biological samples to be recovered at cryogenic temperatures ($T \approx 100$ K) with water being in an amorphous ice state. However, (bulk) water can exist in two amorphous ices at $P < 1$ GPa, low-density amorphous (LDA) ice at low pressures and high-density amorphous ice (HDA) at high pressures; HDA is $\approx 20-25\%$ denser than LDA. While fast/plunge cooling at 1 bar brings the sample into LDA, high-pressure cooling (HPC),

at sufficiently high pressure, produces HDA. HDA can also be produced by isothermal compression of LDA at cryogenic temperatures. Here, we perform classical molecular dynamics simulations to study the effects of LDA, HDA, and the LDA-HDA transformation on the structure and hydration of a small peptide, polyalanine. We follow thermodynamic paths corresponding to (i) fast/plunge cooling at 1 bar, (ii) HPC at $P = 400$ MPa, and (iii) compression/decompression cycles at $T = 80$ K. While process (i) produced LDA in the system, path (iii) produces HDA. Interestingly, the amorphous ice produced in process (ii) is an intermediate amorphous ice (IA) with properties that fall in-between those of LDA and HDA. Remarkably, the structural changes in polyalanine are negligible at all conditions studied ($0 - 2000$ MPa, $80 - 300$ K) even when water changes among the low and high-density liquid states as well as the amorphous solids LDA, IA, and HDA. The similarities and differences in the hydration of polyalanine vitrified in LDA, IA, and HDA are described. Since the studied thermodynamic paths are suitable for the cryopreservation of biomolecules, we also study the structure and hydration of polyalanine along isobaric and isochoric heating paths, which can be followed experimentally for the recovery of cryopreserved samples. Upon heating, the structure of polyalanine remains practically unchanged. We conclude with a brief discussion of the practical advantages of (a) using HDA and IA as a cryoprotectant environment (as opposed to LDA), and (b) the use of isochoric heating as a recovery process (as opposed to isobaric heating).

1 Introduction

Amorphous ice plays a fundamental role in biotechnology. Examples include the cryopreservation of cells, tissues, and organs for storage and subsequent use;[1–4] the study of biological samples, such as proteins, cells, and bacteria, using cryo-electron microscopy (cryo-EM);[5–8] and the determination of protein structures using x-ray diffraction of protein crystals.[9–11] The common features of these techniques are (i) the unavoidable presence of water in the samples of interest, and (ii) the need to reach cryogenic temperatures, $T \approx 100$ K. That water

cannot be avoided in biological samples is not surprising; water is the solvent of life (see, e.g., Ref.[12]). Cells are $> 70\%$ water by weight and all the biochemistry within the cell occurs in an aqueous environment;[13] water is essential in maintaining the stabilization of biologically significant complexes formed by proteins, nucleotides, carbohydrates, and lipids.[13,14]

The need for cryogenic temperatures in biotechnological applications is more subtle. In most cases, including cryopreservation techniques, the use of low temperatures is intended to suppress molecular mobility which may allow for chemical and physical degradation of the sample to be preserved. In the case of x-ray crystallography, cryogenic temperatures also allow for the reduction of radiation damage of protein crystals.[15,16] In cryo-EM, cryogenic temperatures suppress water evaporation of 'unprepared' samples which, otherwise, can damage the EM at room temperatures; as a result, cryo-EM allows for the study of samples in their natural, hydrated state.[17] It is the need to achieve cryogenic temperatures what makes amorphous ice so important: ice formation can be disastrous at $T \approx 100$ K and hence, vitrifying water is the only viable alternative. For example, the formation of extracellular ice can increase the solute concentration in the cell's surroundings[18] which, in turn, can drive the flow of water from inside to outside the cell.[19] It is this change in the solute concentration within the cell that can lead to the cell's death.[19–21] Alternatively, the cell may be depleted of water to such a degree that it collapses, leading to the break down of the cell's membrane.[19] Intracellular ice formation can be equally deadly to the cell.[19,20] In aqueous solutions, changes induced by ice formation can lead to increase in local co-solvents concentrations in the proximity of biomolecules, leading to structural changes such as protein denaturation;[22] ice can destabilize proteins by itself.[23] Briefly, while liquid water is essential to life, ice can be a silent killer. The presence of ice is also undesirable in x-ray diffraction experiments of protein crystals; the x-ray diffraction from ice domains within the sample can affect the quality of the diffraction pattern making it difficult for the determination of protein structures.[9]

Techniques to avoid ice formation in biotechnological applications include the use of

cryoprotectants and additives,[21,24] hyperquenching and rapid cooling (at 1 bar),[21,25,26,28,29] and cooling under pressure.[10,17,30–37] Cryoprotectants, such as low-weight polyols and sugars, and antifreeze proteins can preserve the functionality of biomolecules during cooling and thawing processes and suppress the formation of ice.[19–21] Unfortunately, it is not always evident what kind of additives are needed, and in what amount, to successfully preserve the sample of interest. Cryoprotectants can be toxic[3,22] and, in some cases, they need to be removed after recovery. Since experiments are usually intended to be as non-perturbative as possible, the water content within the sample should not be altered. It follows that in many biotechnological applications, including cryo-EM and x-ray crystallography, the use of cryoprotectants, solvent substitution (e.g., the replacement of water by sugar and small-weight alcohols), and other methods such as chemical fixation, although sometimes necessary, are indeed undesirable.[9,17,31,32,38]

The (out-of-equilibrium) phase diagram of amorphous ice is puzzling.[39–41] Water can exist in two different glassy states at approximately $T < 136$ K ($P < 1000$ MPa), low-density and high-density amorphous ice (LDA and HDA, respectively). LDA and HDA are separated by an out-of-equilibrium first-order phase transition[42] and can be interconverted by, e.g., isothermal compression-decompression and isobaric heating.[43,44] The LDA-HDA transitions are accompanied by remarkably large changes in thermodynamic properties,[40] including density and thermal conductivity; for example, HDA is $\approx 20-25\%$ denser than LDA. LDA and HDA are thought to be the glass counterpart of two liquid states, low-density and high-density liquid water (LDL and HDL), that are separated by a liquid-liquid phase transition (LLPT) ending at a liquid-liquid critical point (LLCP); see, e.g., Ref.[45] That LDA could be obtained by hyperquenching at 1 bar was first discovered by Mayer in 1980.[46] HDA was discovered in 1984 by Mishima *et al.*;[47,48] in 2001, Mishima and Suzuki showed that high-pressure cooling of (emulsified) liquid water produces HDA.[49] Surprisingly, most studies using high-pressure cooling in x-ray protein crystallography experiments have overlooked at the fact that vitreous water can exists in two amorphous ice states; the work from Grunner

and collaborators being an exception.[9,35,50] To the best of our knowledge, there is no reference to HDA in studies using high-pressure cooling for cryo-EM and cryopreservation applications.

The complex phase diagram of supercooled and glassy water raises fundamental questions relevant to the biotechnological techniques mentioned above. For example, what are the roles of LDA and HDA in the preservation of biological samples, including biomolecules, cells, and bacteria, at cryogenic temperatures? Can biomolecules survive the heating-induced HDA-to-LDA transformation? In this work, we address these questions by studying the behavior of a small peptide along the thermodynamic paths shown in Fig. 1. Path (A) in Fig. 1(b) corresponds to the hyperquenching of liquid water at 1 bar to produce LDA.[25,26,46] Path (B) in Fig. 1(c) corresponds to the isobaric cooling of water under pressure, followed by decompression at low temperatures.[51] Path (C) in Fig. 1(d) corresponds to a compression/decompression cycle at $T = 80$ K and $0 < P < 2000$ MPa which leads to the LDA-to-HDA transformation of bulk water. Included in Figs. 1(c) and 1(d) is the LLPT and LLCP of *bulk* water. Accordingly, it is *expected* that path (B) and (C) will lead to the formation of HDA within the sample. The recovery of the sample from paths (A), (B), and (C) are performed by isobaric heating at normal pressure (red arrows). Upon isobaric heating, HDA transforms to LDA at $T \approx 115$ K (pure water) and hence, LDA is unavoidable before the system reaches the liquid state. Accordingly, we also explore the behavior of polyalanine along the isochoric heating runs indicated by the green arrows in paths (B) and (C) [only]. Along these paths, LDA and the ices may be avoided altogether. The exploration of the isochoric heating of polyalanine-HDA samples is inspired in the recent experiments of Ref.[52] involving laser-induced hyperheating techniques. As discussed in that work, fast laser-induced heating runs are, effectively, isochoric heating processes and hence, isochoric heating is, nowadays, experimentally feasible. Accordingly, we propose here to employ isochoric heating of samples vitrified in high-density amorphous ices as a novel method to avoid crystallization in cryopreservation techniques. This is because the structure of high-density amorphous ices is incompatible to that of ice Ic/Ih and hence, HDA is less prompt to crystallization (into

Ih/Ic) than LDA. Our study is based on MD simulations of a polyalanine peptide, composed of 20 residues, immersed in water [Fig. 1(a)]. As shown below, the secondary alpha (helical) structure of polyalanine remains practically unchanged along the thermodynamic paths (A)-(C) explored, even when water transforms among the low- and high-density liquids, LDA, and/or HDA states. We also describe in detail the hydration of polyalanine and find that the presence of polyalanine tends to suppress the formation of HDA. The role of the protocol followed in the preparation of the sample in the glass state is also discussed.

This work is organized as follows. In Sec. 2 we present the computer simulations details. The results are included in Sec. 3 where we discuss the structure and hydration of polyalanine along the thermodynamic paths indicated in Fig. 1. A summary is included in Sec. 4.

2 Computer Simulation Details

We perform out-of-equilibrium molecular dynamics (MD) simulations of a system composed of $N = 6857$ water molecules and one 20-residues polyalanine peptide with an alpha helical secondary structure; see Fig. 1(a). The α-helical polyalanine was capped with an acetyl group in the N-terminus, while the C-terminus was capped with an NH_2 group. The peptide is ≈ 3.2 nm long and the (cubic) box side length is at least 5.9 nm at all conditions studied. Periodic boundary conditions are applied along all three directions. Polyalanine is modeled using the CHARMM36 force field[53] and water molecules are represented using the TIP4P/2005 model.[54]

We perform equilibrium MD simulations at (i) $P = 0.1$ and 400 MPa for $T = 400$, 375, 350, 325, 300, 280, 260, 240, and 220 K; and (ii) $T = 240$ K for $P = 50,\ 100,\ 150, ...,\ 400$ MPa. The MD simulations are run for 50 ns at $T > 300$ K and 100 ns at $T \leq 300$ K using a simulation time step of 2 fs. The equilibrium simulations at $T = 240$ K and $P = 0.1,\ 400$ MPa are the starting point for the out-of-equilibrium simulations indicated in Fig. 1(b)-(d) (states A and A').

We performed four kinds of out-of equilibrium MD simulations: (a) isobaric cooling runs [vertical blue arrows in Fig. 1(b)(c)]; (b) isothermal compression/decompression runs [horizontal blue, violet, and magenta arrows in Fig. 1(c) and 1(d)]; (c) isobaric heating runs [vertical red arrows in Fig. 1(b)-(d)]; and (d) isochoric heating runs [green arrows in Fig. 1(c) and 1(d)]. We follow the same protocol employed in Ref.[55–58] for the case of glassy (bulk) TIP4P/2005 water. During the cooling and heating runs, the thermostat temperature is changed linearly with time with a cooling/heating rate of $q_T = 1$ K/ns; the volume or barostat pressure is maintained constant depending on the path followed in Fig. 1(b)(c). The cooling rates employed in this work are faster than those employed in micro-EM and fast-quenching/plunge cooling experiments ($q_T = 0.01 - 0.001$ K/ns).[26,27] A recent study exploring the effect of rates in computer simulations of bulk glassy water indicates that reducing the rates leads to relatively minor quantitative changes but the qualitative phase behavior of glassy water remains unaltered.[57] During isothermal compression/decompression, the thermostat temperature is maintained constant while the pressure is increased/decreased in steps of $\Delta P = 10$ MPa. At each pressure, the MD simulation is run for $\Delta t = 1$ ns, resulting in a compression/decompression rate of $q_P = 10$ MPa/ns. To take into account fluctuations in the results due to differences in the starting configurations, we perform five independent runs for each of the thermodynamic paths shown in Fig. 1.

Simulations are performed using the GROMACS software package.[59] A cutoff $r_c = 1.1$ nm is used to calculate the Lennard-Jones interactions. Electrostatic interactions are treated using the Particle-Mesh Ewald (PME) method with the same cutoff $r_c = 1.1$ nm. The temperature and pressure are controlled using a Nose-Hoover thermostat and a Berendsen barostat.

3 Results

In Sec. 3.1, we discuss the structure and hydration of polyalanine during vitrification by hyperquenching at (i) $P = 0.1$ MPa, into LDA, as well as at (ii) $P = 400$ MPa. We also discuss the structure and hydration of polyalanine in the HDA form prepared by isothermal compression of the system from $P = 0.1$ MPa to $P = 2000$ MPa, followed by decompression back to $P = 0.1$ MPa. In Sec. 3.2, we discuss how polyalanine, vitrified in the different amorphous ices, can be recovered by isobaric or isochoric heating runs.

3.1 Vitrification at $P = 0.1$ and 400 MPa

3.1.1 Amorphous Ice

Fig. 2(a) shows the density of the polyalanine-water system upon cooling at $P = 0.1$ MPa from $T = 240$ K (state A) to $T = 80$ K (state B). For comparison, we also include in Fig. 2(a) the density of *bulk* water during identical cooling runs (from Ref.[56]). The case of pure water is discussed in detail in Ref.[56] Briefly, at high temperatures (approximately $T \geq 200$ K), the density of water during the cooling process ($q_T = 1$ K/ns) practically matches the equilibrium densities (open blue circles). Upon cooling at $T < 200$ K, water vitrifies and forms LDA. In the LDA state, $\rho(T)$ increases linearly upon cooling (dashed lines). It follows from Fig. 2(a) that water enters the LDA state at approximately $T = 180$ K for the case of $q_T = 1$ K/ns.

A similar picture holds for the polyalanine-water system [Fig. 2(a)]. Specifically, $\rho(T)$ increases linearly upon cooling at low temperatures, where the polyalanine-water system is in a glassy state, and it varies non-linearly with T at higher temperatures, while the system is in the equilibrium liquid state (open red circles). The liquid-to-glass transition occurs approximately at $T = 210$ K ($q_T = 1$ K/ns). This suggests that the presence of polyalanine tends to slow down the dynamics of water, increasing the vitrification temperature of the system relative to bulk water. The shift in the liquid-to-glass transition is consistent with the corresponding shift in the maximum density temperature; the maximum density temperature

in the water-polyalanine system is $\approx 20 - 30$ K higher than in bulk water [open blue and red circles in Fig. 2(a)]. We also note that, not surprisingly, the density of the polyalanine-water system is larger than the density of bulk water. Yet, as one would expect, water within the polyalanine-water system forms predominantly LDA at low temperatures. This is confirmed by the water OO radial distribution function (Ow-Ow RDF) shown in the inset of Fig. 2(c).[60] Specifically, the RDF of water in the polyalanine-water system at $T = 80$ K and $P = 0.1$ MPa (state B; red line) is very similar to the RDF of bulk LDA reported in Ref.[56] at same conditions (violet line). The main characteristic in the structure of LDA is the presence of a wide empty interstitial space at $r \approx 0.35$ nm, where its RDF is zero, and a second hydration shell at $r \approx 0.45$ nm. As one would expect, the Ow-Ow RDF in state B (LDA) is reminiscent to the RDF of its parent liquid at $T = 240$ K and $P = 0.1$ MPa (LDL-like state A); see the main panel of Fig. 2(c).

Fig. 2(b) shows the density of the polyalanine-water system during HPC at $P = 400$ MPa. As for the case of $P = 0.1$ MPa, the system enters the glass state at $T \approx 170$ K, below which $\rho(T)$ increases linearly upon further cooling. At high temperatures, the system samples equilibrium states and its density varies non-linearly with T; at these temperatures, the density of the system during the HPC process matches the density of the equilibrated liquid (open red circles). There is no anomalous density maximum at $P = 400$ MPa.

As indicated schematically in Fig. 1(c), the water component of the polyalanine-water system at $T = 80$ K and $P = 400$ MPa (state B') is *expected* to be in the HDA state since the pressure of the LLCP in *bulk* TIP4P/2005 water is at much smaller pressure, $P_c = 185$ MPa.[61] That water in state B' is in an HDA form is consistent with the large density of the water-polyalanine system at these conditions, $\rho = 1.19$ g/cm^3, which is ≈ 17 % larger than the density of the polyalanine-water system prepared at $T = 80$ K and $P = 0.1$ MPa (state B), $\rho = 1.015$ g/cm^3. However, some structural properties of amorphous ice in state B', such as water coordination number, are closer to the corresponding properties of LDA (see Sec. 3.1.3). Other structural properties, such as the Ow-Ow RDF, are intermediate between

those of LDA and HDA. The Ow-Ow RDF of the polyalanine-water system in state B' is shown in Fig. 2(c) (green line). Compared to the RDF in state B, the Ow-Ow RDF in state B' has a smaller second maximum at $r \approx 0.43$ nm and a larger value at $r \approx 0.35$ nm. This implies that, relative to state B, the water molecules of the system in state B' have a more distorted second hydration shell with some molecules populating the first interstitial shell at $r \approx 0.35$ nm. Analogous structural changes in the Ow-Ow RDF are known to occur during the LDA-to-HDA transformation of bulk water.[62] Yet, as we discuss below, the interstitial space of amorphous ice in state B' remains mildly populated compared to bulk HDA. For these reasons, we will not identify the amorphous ice produced in state B' as LDA or HDA but as an 'intermediate' amorphous ice (IA). As we show in Sec. 3.1.3, IA is a homogeneous amorphous ice composed of water molecules with $n = 4$ nearest-neighbors, reminiscent to LDA-like molecules, and molecules with $n > 4$, reminiscent to HDA-like molecules. This is somewhat different from the picture suggested in Refs.,[35,50] where HPC of aqueous protein crystals was interpreted as producing HDA.

From the experimental point of view, samples are usually brought to $P = 0.1$ MPa for analysis and/or storage. Hence, we also decompressed the polyalanine-water system prepared by HPC at $P = 400$ MPa to $P = 0.1$ MPa [B'-to-B" arrow in Fig. 1(c)]. The density of the system during decompression is indicated by the green line in Fig. 3. During decompression from state B' to B", the density of the system decreases linearly from $\rho \approx 1.19$ g/cm^3 at $P = 400$ MPa to $\rho \approx 1.15$ g/cm^3 at $P = 0.1$ MPa. Hence, the density of the system at state B" remains somewhat high, 13 % larger than the density of the system in state B. This suggests that, as expected, polyalanine in state B" remains vitrified in an IA. Indeed, as shown in Fig. 2(c), the Ow-Ow RDF of water in states B' and B" exhibit minor differences. Interestingly, Fig. 3 indicates that further decompression of the polyalanine-water system is possible down to very low pressures, $P = -800$ MPa ($T = 80$ K), below which the polyalanine-water glass fractures.

Next, we show that the IA produced at $P = 0.1$ MPa and $T = 80$ K [Fig. 1(c)] is slightly

different from the HDA produced at the same conditions by the compression/decompression cycle of Fig. 1(d). Fig. 3 shows the density of the polyalanine-water system along the path indicated in Fig. 1(d) (violet and magenta arrows). During compression at $T = 80$ K, a sudden densification occurs at $P \approx 1200$ MPa which signals the LDA-to-HDA transformation of the water component in the system. At $P = 2000$ MPa (state X), polyalanine is trapped in an HDA form and the system reaches a large density of $\rho = 1.41$ g/cm^3. Upon decompression from $P = 2000$ MPa to $P = 0.1$ MPa, polyalanine remains in an HDA environment and the system density decreases to $\rho = 1.21$ g/cm^3. The main point of Fig. 3 is that the densities of the glassy polyalanine-water system produced by HPC (green line) and by isothermal compression/decompression (blue lines) differ. In particular, the density of the polyalanine-IA system in state B" and polyalanine-HDA system in state Y are $\rho = 1.15$ and $\rho = 1.21$ g/cm^3, respectively. It follows that the amorphous ices hosting polyalanine depends on the preparation process employed [Fig. 1(c) and 1(d)]. This can have important implication if the sample needs to be recovered at room temperature; see Sec. 3.2. That the IA and HDA are different is also indicated by the corresponding Ow-Ow RDF; see Fig. 4. These RDFs differ mainly in their values at the locations corresponding to water's second hydration shell ($r \approx 0.45$ nm) and first interstitial shell ($r \approx 0.35$ nm). Briefly, water molecules in state Y have (i) a more populated first interstitial shell and (ii) a less pronounced second hydration shell than water molecules in state B". It is this enhanced collapse of water's second hydration shell that leads to a larger density of the system in state Y. Fig. 4 also shows that the Ow-Ow RDF of the IA is indeed intermediate between the RDF of LDA (state B) and HDA (state Y).

We conclude this section by comparing the HDA form produced in the water-polyalanine system by compression/decompression at $T = 80$ K [Fig. 1(d)] with the HDA produced in bulk water under the same thermodynamic path. The density of the water-polyalanine system along the compression/decompression cycle is shown in Fig. 3 (blue lines) together with the corresponding density of bulk water (dashed black lines, from Ref.[56]). Interestingly,

the presence of polyalanine shifts the pressure-induced LDA-to-HDA transformation pressure from $P_{L-H} \approx 850$ MPa (bulk water, dashed lines) to $P_{L-H} \approx 1200$ MPa (polyalanine-water, blue lines). Fig. 4 shows the Ow-Ow RDF of the water-polyalanine system at state Y together with the corresponding RDF of bulk HDA at the same conditions, $P = 0.1$ MPa and $T = 80$ K [the same preparation process, with identical cooling/compression/decompression rates were employed]. Relative to state Y, the Ow-Ow RDF of water in the bulk HDA is characterized by the absence of a maximum (at $r \approx 0.43$ nm) and the presence of a maximum within the first interstitial space (at $r \approx 0.35$ nm). Hence, water molecules in bulk HDA have a denser environment with more neighbors in their first interstitial shell. This suggest that, from the point of view of water structure, the effective pressure of water in the water-polyalanine system is lower than the real pressure P of the system. Consistent with this, we note that the Ow-Ow RDF of the system at state B", at $P = 400$ MPa and $T = 80$ K, is practically identical to the Ow-Ow RDF reported in Ref.[62] for bulk HDA obtained by HPC at $P = 200$ MPa and $T = 80$ K.

3.1.2 Polyalanine Structure

Next, we focus on the structure of polyalanine. As shown in the SM, polyalanine denatures at $T > 300$ K at both $P = 0.1$ and 400 MPa. Yet, we find that α-helical polyalanine structure is maintained along all the thermodynamic paths indicated in Figs. 1(b)-(d). To show this, we include in Fig. 5 the Ramachandran plots for polyalanine in states A, B, A', B', B", X, and Y. The characteristic values of the dihedral angles ψ and ϕ for a right-handed alpha helix peptide are $\psi \approx (0, -60)^0$ and $\psi \approx (-30, -180)^0$. It follows from Fig. 5 that the structure of polyalanine corresponds to an alpha helix. There are a few amino acids that seem to exhibit minor structural deviations from the alpha helix structure, with $\psi > 0^0$. We find that these dihedral angles are associated to the $1-2$ amino acids located at the end terminals of polyalanine. We also compare different structural properties of polyalanine in states A, B, A', B', B", X, and Y. Specifically, included in Table 1 are polyalanine radius of

gyration R_g, length L_p, number of internal hydrogen-bonds (n_{HB}), average distance between nearest-neighbor C_α atoms $d_{C\alpha C\alpha}$, as well as the solvent accessible surface area (SASA). It follows from Table 1 that all these properties barely change among states A, B, A', B', B", X, and Y. In particular, the values of n_{HB} and SASA in these states are very different from those in the denatured states (see SM).

We stress that the lack of structural changes in polyalanine, as it is driven among the states A, B, A', B', B", X, and Y, is not necessarily what may be expected. These states differ by up to 2000 MPa in pressure and 160 K in temperature. In particular, the state of water changes drastically among these states, from the liquid state (LDL-like in state A; HDL-like in state A') to LDA (state B), IA (states B', B"), and HDA (states X, Y). Accordingly, water dynamic (e.g., diffusivity), structural (e.g., RDF, tetrahedral order), and thermodynamic properties (e.g., density, compressibility) vary considerably as well.[55] Yet, polyalanine remains structurally indifferent to such variations. The changes among LDA, IA, and HDA are, after all, related to profound changes in the water-water hydrogen-bonds (HB). Yet, the internal HB of polyalanine, which are responsible of its alpha helix structure, are not affected along the thermodynamic paths explored.

3.1.3 Polyalanine Hydration

A natural question follows, what are the changes in the hydration of polyalanine as the system evolves among states A-B, A'-B'-B", and B-X-Y? To address these questions, we take advantage of the helical structure of polyalanine and calculate cylindrical distribution functions (CDF). To calculate a given CDF, we first identify the axis of polyalanine. Specifically, we split polyalanine into two ('upper' and 'lower') halves. We then identify the coordinates of the center of mass of the ten C_α atoms of the upper half of polyalanine ($R_{CM,u}$); similarly, we also calculate the coordinates of the center of mass of the ten C_α atoms of the lower half of polyalanine ($R_{CM,l}$). The axis of polyalanine is the line that passes through points $R_{CM,u}$ and $R_{CM,l}$. The water CDF measures distributions of Ow atoms as function of their distance

d to polyalanine's axis. We include the total CDF as well as the CDF of water molecules with different numbers of nearest-neighbors (NN) n within a cutoff distance $r_c = 0.34$ nm. The value $r_c = 0.34$ nm is chosen because it is the maximum cutoff distance that gives, in average, $n = 4$ for the system in states A and B (see SM) where water is in LDL-like and LDA states. The value $r_c = 0.34$ nm has also been used in experimental studies to quantify the coordination number in high-density amorphous ices.[63] The CDF for molecules with n NN are somewhat sensitive to the value of r_c. Hence, for comparison, we also include in the SM the CDF calculated using $r_c = 0.32$ nm, which corresponds to the first minimum of the Ow-Ow RDF in LDA ($T = 80$ K and $P = 0.1$ MPa).

Figs. 6(a) and 6(b) show the CDF of Ow atoms when the system is in states A and B, respectively [see Fig. 1(b)]. In state A, water molecules are in an LDL-like state and have mostly $n = 3$ (black line) and $n = 4$ (red line) NN. A small number of 'residual' water molecules with $n = 5$ (green line) are also found (≈ 7 % of all the water molecules in the system). Not surprisingly, molecules with $n = 3$ NN are predominantly in contact with polyalanine, $d \approx 0.35 - 0.7$ nm. Indeed, as shown in Fig. 6(f), the CH_3 side chains of polyalanine, which are located in the outer surface in contact with water, extend up to $d \approx 0.5$ nm. At $d > 0.7$ nm, most water molecules (> 90 % of all the water molecules in the system) have $n = 4$ NN consistent with water being in an LDL-like state. Interestingly, a first (cylindrical) shell can be approximately identified at $d \approx 0.35 - 0.75$ nm (extending up to the first minimum of the CDF, at $d \approx 0.75$ nm). The effects of vitrifying the system at $P = 0.1$ MPa on the CDF are mild. As shown in Fig. 6(b), vitrification reduces considerably the number of 'residual' water molecules with $n = 5$ NN and increases slightly the fraction of interfacial water molecules with $n = 3$. Briefly, relative to bulk water, corresponding to approximately $d > 1.5$ nm, polyalanine in the LDA state has a hydration shell with a mild excess of water molecules mostly with $n = 3$ and $n = 4$ NN.

The CDF of water in the HDL-like state A' is shown in Fig. 6(c). Upon compressing the system from state A ($P = 0.1$ MPa) to state A' ($P = 400$ MPa) at $T = 240$ K, the first

maximum of water CDF becomes slightly thinner and larger. Specifically, the first minimum of the total CDF shifts from $d = 0.75$ nm in state A to $d = 0.65$ nm in state A', and the first maximum of the total CDF increases from ≈ 1.3 in state A to ≈ 1.4 in state A'. Hence, as expected, polyalanine is surrounded more tightly by its interfacial water layer. The main feature of state A' is the relative large number of water molecules with $n \geq 5$ NN which is indicative that polyalanine is in an HDL-like state. At $d > 1.5$ nm, corresponding to bulk water, ≈ 70 % of the water molecules have $n \geq 5$ NN, the remaining water molecules having $n = 4$ NN. However, as d decreases below 1 nm, the number of water molecules with $n = 4$ increases while less molecules are found with $n \geq 5$ NN. Hence, compared to bulk water ($d > 1.5$ nm), the interface of polyalanine is depleted of molecules with $n \geq 5$ and contains a larger number of molecules with $n = 4$ NN; similar results hold for $r_c = 0.32$ nm (see SM). In addition, relative to state A, polyalanine hydration layer in state A' is composed of a smaller number of water molecules with $n = 3$ NN and a larger number of water molecules with $n = 5$ NN.

The effects of HPC the water-polyalanine system at $P = 400$ MPa are relevant. A comparison of the total CDF in Figs. 6(c) and 6(d) shows that HPC leads to more distinguishable (cylindrical) hydration shells around polyalanine. The first maximum of the total CDF increases from 1.4 to 1.7 meaning that the hydration layer of polyalanine becomes considerably denser upon cooling. In addition, the number of water molecules with $n \geq 5$ NN decreases leading to an increase of molecules with $n = 4$ NN. Remarkably, the hydration layer of polyalanine ($d < 0.65$ nm), is mostly depleted of water molecules with $n = 5$ NN. Instead, there is a large fraction of water molecules with with $n = 4$ NN and, of course, water molecules with $n = 3$ NN (in contact with polyalanine). Our results show that polyalanine in state B' is tightly surrounded by mostly LDA-like water molecules since these molecules have $n \leq 4$ NN. However, these molecules may have $n < 5$ NN just because of geometric constraints. Specifically, water molecules within polyalanine hydration layer ($d \leq 0.65$ nm) are within a distance ≈ 0.3 nm from polyalanine. Hence, independently of polyalanine sur-

face chemistry, interfacial water molecules have a smaller available space to accommodate NN within a distance $r_c = 0.34$ nm. A classification of hydration water molecules as LDA or HDA may be misleading since these molecules belong to the polyalanine-water *interface* and hence, may have very different properties from bulk water.[64] In the bulk water region ($d > 1.5$ nm), 30 % and 70 % of the water molecules in the system have, respectively, $n \geq 5$ (HDA-like) and $n = 4$ (LDA-like) NN (similar conclusions follow for the case $r_c = 0.32$ nm; see SM). It may be unexpected that only $\leq 30\%$ of the water molecules in the amorphous ice formed in state B' can be classified as HDA ($n \geq 5$ NN). If the amorphous ice in state B' was HDA, the majority of the water molecule should be highly coordinated, with $n \geq 5$ NN. This is one of the reasons why we identify amorphous ice in state B' as IA, instead of HDA (similar conclusions follow for the case $r_c = 0.32$ nm; see SM).

The effects of decompressing the system from $P = 400$ MPa (state B') to $P = 0.1$ MPa (state B") are negligible. The CDFs in Figs. 6(d) and 6(e) are barely distinguishable. Accordingly, at $P = 0.1$ MPa and $T = 80$ K, independently of whether bulk water forms LDA (state B) or IA (state B"), the first hydration layer of polyalanine is composed mostly of low-coordinated molecules with $n \leq 4$ NN. However, the hydration layer in state B" is thinner and much denser than in state B.

Next, we discuss briefly the hydration of polyalanine in states B" and X-Y. The water CDF in states X and Y are shown in Figs. 7(a) and 7(b). The high density of the polyalanine-water system in state X ($\rho = 1.41$ g/cm^3) is consistent with the large number of water molecules with $n = 5-9$ NN; no water molecules have $n = 4$ NN at $d > 1.5$ nm. Experiments also find that in high-density forms of amorphous ice, water molecules may be found with large numbers of NN, e.g., $n = 5 - 8$ at $P = 0.1$ MPa for $r_c \leq 0.35$ nm.[63] It also follows from Fig. 7(a) that the first hydration shell of polyalanine ($d = 0.35 - 0.65$ nm) is composed of a large number of HDA-like molecules with $n = 5$ NN. Hence, it is remarkable that the structure of polyalanine remains unaffected at state X where $P = 2000$ MPa (Sec. 3.1.2).

Decompression of the system from state X to state Y ($P = 0.1$ MPa), has also important

effects. In the bulk water region ($d > 1.5$ nm), removing pressure decreases considerably the number of water molecules with $n \geq 7$ at the expense of increasing the fraction of water molecules with $n = 4,\ 5,\ 6$. In the bulk, only $\approx 25\%$ of all the water molecules in the system have $n = 4$ NN which is consistent with the expectations of an HDA state where most water molecules should have $n \geq 5$ NN. Interestingly, the total CDF in state Y [magenta line in Fig. 7(b)] is more reminiscent to the total CDF in the LDA state B [Fig. 6(b)] than in the HDA state B" [Fig. 6(e)]. However, the first hydration layer of polyalanine in state Y contains a large fraction of water molecules with $n = 5$ NN (but most water molecules at the interface of polyalanine still have only $n = 4$ NN).

Summarizing, polyalanine in state B, B", and Y, while being at same conditions $P = 0.1$ MPa and $T = 80$ K, is hydrated by different environments. In state B, bulk water is in the LDA state; in states B" and Y, bulk water is in IA and HDA states, respectively. These amorphous ices are characterized by water molecules with very different coordination numbers. Yet, in all three cases, polyalanine hydration layer is composed mostly of water molecules with $n = 4$ NN; molecules with $n = 3$ NN are only found in contact with polyalanine. In particular, only in the case of polyalanine vitrified in HDA (state Y), the hydration layer of water has a relevant fraction of HDA-like molecules with $n = 5$ NN.

3.2 Recovery of Polyalanine upon Heating

In many biotechnological applications, including cryo-EM and x-ray protein crystallography, the sample at cryogenic temperatures does not need to be recovered. Recovery of the sample is necessary in the cryopreservation of biomolecules at low temperatures. In Sec. 3.2.1, we explore briefly how water and polyalanine evolve as the system in states B, B", and Y is heated at constant pressure ($P = 0.1$ MPa). Experimentally, isobaric heating of cryopreserved samples at $P = 0.1$ MPa can be problematic due to the rapid crystallization of water into hexagonal (Ih) and cubic ice (Ic). As shown in Figs. 1(b)-(d) [red arrows], heating amorphous ices at normal pressure bring the systems through the domain of these low pressure

ices. Crystallization can be avoided by using fast heating rates or by using cryoprotectants.

In Sec. 3.2.2, we discuss how water and polyalanine evolve as the system in states B" and Y is heated at constant volume. This heating process is motivated by recent experiments,[52] showing that HDA, recovered at $P = 0.1$ MPa and cryogenic temperatures, can be heated *isochorically* by using short (100 fs) IR laser pulses. The heating rate in these experiments is extremely fast, even for the time scales of MD simulations ($q_T \approx 1000$ K/ns), and hence, there is no time for the volume of the system to vary during the heating process. MD simulations and experiments[52] show that by heating HDA at constant volume, the pressure of the sample increases with increasing temperature and the thermodynamic path followed by the system is alike the green arrows in Fig. 1(c)(d); these thermodynamic paths pass below the location in the P-T plane of *bulk* water LLCP. Accordingly, upon isochoric heating, biomolecules trapped in an IA or HDA matrix (state B" and Y) should avoid the region in the P-T plane where crystallization to ice Ih/Ic occurs. For example, the density of (bulk) HDA at $P = 0.1$ MPa is $\rho_{HDA} > 1.15$ g/cm^3 which is incompatible with the density of ice Ih and Ic (for example, the density of ice Ih is $0.917 - 0.934$ g/cm^3 at $T = 93 - 273$ K and $P = 0.1$ MPa).

3.2.1 Isobaric Heating at $P = 0.1$ MPa

Fig. 8 shows the density of the polyalanine-water system upon heating at $P = 0.1$ MPa. The glassy samples are initially in state B, where water is in an LDA-like state, and states B" and Y, where water is in IA and HDA-like states, respectively. In all three cases, the densities overlap at approximately $T \geq 240 - 250$ K indicating that at these temperatures, the systems are already in the equilibrium liquid state ($q_T = 1$ K/ns). Instead, at low temperatures, the density of the systems differ considerably. As observed in the case of bulk TIP4P/2005 glassy water,[55,56] the density of the sample recovered at state B remains low at all temperatures since, in this case, amorphous ice is in the LDA state and LDA transforms directly to LDL upon heating. In the case of the water-polyalanine systems containing

IA and HDA forms (states B" and Y), the density decreases rapidly upon heating at low temperatures. This is because, at $P = 0.1$ MPa, HDA and IA transform to LDA or LDL upon heating. For example, in the case of bulk water, heating HDA at normal pressure produces LDA which then reaches the glass transition upon further heating. However, in the case of TIP4P/2005,[55,56] the HDA-to-LDA transformation is difficult to identify at the fast rate $q_T = 1$ K/ns (see Refs.[55,56] for details). The HDA-to-LDA transformation is clearly detected in ST2 water[65] because the LLCP in ST2 water is at much higher temperature than in TIP4P/2005 water, allowing for the detection of the HDA-to-LDA transition at faster heating rates.

The behavior of $\rho(T)$ in Fig. 8 suggests that the glass transition in the three systems studied is approximately $T_g = 220 - 240$ K ($q_T = 1$ K/ns). This is consistent with the corresponding T-dependence of the isobaric heat capacity $C_P(T)$ and with the mean-square displacement of the water molecules as function of temperature, $MSD(T)$; see SM.

As found during vitrification, the structure of polyalanine remains practically unaffected upon isobaric heating, even when water evolves among the LDA, HDA, and LDL states. Tables S1-S3 in the SM shows specific properties of polyalanine at selected temperatures during the heating runs shown in Fig. 8.

3.2.2 Isochoric Heating of Polyalanine-HDA Samples

Fig. 9 shows the pressure of the polyalanine-water systems prepared at $T = 80$ K in the states (a) B" ($\rho = 1.15$g/cm^3) and (b) Y ($\rho = 1.21$g/cm^3), during isochoric heating. We include results obtained with heating rates $q_T = 1 - 1000$ K/ns since the experimental heating rate is $q_T \approx \mathcal{O}(1000)$ K/ns. The behavior of $P(T)$ is similar in both samples studied. Specifically, at high temperatures, the pressure of the system is independent of q_T since the system is sampling the equilibrium liquid states. At low temperatures, the $P(T)$ increases rapidly with increasing temperature and reaches the liquid state at different glass transition temperatures. T_g decreases with decreasing cooling rates and it is, approximately, in the

range $170 < T_g < 240$ K ($205 < T_g < 290$ K) for the system starting in state Y (B"). As shown in the SM, these values of T_g are consistent with the behavior of the total energy, constant-volume heat capacity $C_V(T)$, and $MSD(T)$ upon heating; see SM.

An important point follows from Fig. 9. Specifically, the pressure of the water-polyalanine system, recovered in the liquid state, depends strongly on the specific amorphous ice formed within the sample (IA in state B"; HDA in state Y). For example, at $T \approx 200$ K, $P \approx 350 - 400$ MPa for the system originally in state B", while $P \approx 500 - 600$ MPa for the system originally in state Y. This has important practical implications. If the system reaches very high pressures after recovery, molecular changes may occur in the biological sample to be preserved; e.g., most proteins denature in the range $200 - 700$ MPa.[66] Fig. 9 indicates that the density of the amorphous ice matrix hosting the biomolecule (at $T = 80$ K) defines the pressure that the sample will reach after isochoric heating. In particular, by forming an amorphous ice of 'low' density within the sample (but denser than LDA), such as IA, it may be possible to use the recipe defined in Fig. 1(c) to store-and-recover biomolecules at cryoprotectant temperatures (while avoiding ice formation).

4 Summary and Discussion

In this work, we explore the behavior of polyalanine immersed in water along the thermodynamic paths described in Fig. 1(b)-(d) where water is vitrified into different amorphous ices. While the process in Fig. 1(b) vitrifies water into LDA; the process in Fig. 1(d) vitrifies water into HDA. Interestingly, the amorphous ice produced in the process shown in Fig. 1(c), IA, was shown to have a density and structural properties that are intermediate between those of LDA and HDA. Remarkably, the structural changes in polyalanine are negligible at all conditions studied ($0 - 2000$ MPa, $80 - 300$ K) even when water changes among the low and high-density liquid states, LDA, IA, and HDA (note that polyalanine was found to denature at $T > 300$ K for $P = 0.1,\ 400$ MPa). Our study is meant to provide a molecular level

understanding of the structure of biomolecules in different amorphous ices which is relevant in biotechnological applications, including cryo-EM, x-ray protein crystallography, and in the cryopreservation of small biological samples and molecules. An interesting and important topic that deserves further inquiry is whether biomolecules possessing greater structural complexity than polyalanine are also insensitive to the nature of the glassy matrix (LDA vs HDA) or the thermodynamic path undertaken.

An important implication of this study is that one should be careful in using the 'phase diagram' of glassy water, which includes LDA, HDA, LLPT and a LLCP, to interpret experiments of biomolecules in amorphous ices (see, e.g., Refs.[35,50]). For example, we find that the inclusion of just one 20-residue polyalanine peptide in $N = 6857$ water molecules can shift the vitrification temperatures and density maximum temperature by $20 - 30$ K at $P = 0.1$ MPa [Fig. 2(a)], and increase the pressure-induced LDA-to-HDA transformation pressure by ≈ 350 MPa at $T = 80$ K [Fig. 3]. This suggests that the location of the LLPT, LLCP, and LDA/HDA domains in the P-T plane of bulk water may be shifted considerably even if the solution is highly diluted (see also Ref.[62,67]). The implications of this finding are important for cryopreservation applications. For example, while HPC of bulk water at $P = 400$ MPa produces an HDA-like state, we find that instead, in the presence of polyalanine, the same process brings water into an IA. Indeed, the Ow-Ow RDF of IA at $P = 400$ MPa is practically identical to the RDF of bulk water at $P \approx 200$ MPa ($T = 80$ K). We note that the change in the phase diagram of glassy water in the presence of solvents implies that the amorphous ice formed at a specific (T, P) conditions, by a given preparation path, is not unique and may vary depending on the solutes involved and their concentration.

Our study also shows the important role of amorphous ice in the hydration of polyalanine. As shown in Figs. 6 and 7, the hydration shell of polyalanine is very different depending on whether water forms LDA, HDA, and IA; for example, the thickness and local density of polyalanine hydration shell varies considerably depending on whether polyalanine is hosted by LDA, HDA, and IA. In addition, the local structure of water surrounding polyalanine

differs as well. While water molecules have mostly $n \leq 4$ nearest-neighbors in the hydration shell of polyalanine vitrified in LDA and IA, there is a relevant fraction of HDA-like water molecules ($n \geq 5$) in the hydration shell of polyalanine vitrified in HDA.

The nature of the amorphous ice hosting a given biomolecule, such as polyalanine, cannot be overlooked, i.e., not all amorphous ices are the same. This is particular relevant if the sample is recovered by isochoric heating [Fig. 9]. In these cases, the pressure reached by the sample after recovery, in the liquid state, depends directly on the density of the amorphous ice present. We find that the higher the density of the amorphous ice surrounding polyalanine, the larger the pressure of the system after recovery. In particular, for the polyalanine-HDA system, the pressure of the sample is $P = 500 - 600$ MPa after recovery. These values of pressures may induce denaturation in real proteins.

In this work, we proposed to use (a) isochoric heating of (b) samples cryopreserved in IA and HDA forms as an advantageous process for recovery. Isochoric heating of amorphous ice is possible by using short IR laser pulses.[52] In our computer simulations, polyalanine was first vitrified at $T = 80$ K and $P = 0.1$ MPa in an IA and HDA matrix and, then, the system was heated at constant density. In both cases, we found no structural changes in polyalanine, suggesting that rapid isochoric heating may be harmless to biomolecules. The advantage of this process, relative to iso*baric* heating, is that the pressure of the system increases rapidly during isochoric heating. As shown schematically in Figs. 1(c)-(d) [see also Fig. 9], the thermodynamic path followed by the system in the P-T plane passes below the location of the LLCP of *bulk* TIP4P/2005 water and hence, away from the stability region of ice Ih and Ic. It is hence possible that ice formation is avoided. Indeed, in the experiments of Ref.[52] with bulk water, ice formation was not observed during the isochoric heating process. In practice, one could apply a laser pulse that brings the cryopreserved sample to liquid temperatures, $T > 240$ K (isochorically). As shown in Ref.,[52] the pressure of the sample decreases rapidly to 1 bar soon after the laser pulse ends.

The isochoric heating process is probably useful only if the biomolecule to be preserved

is vitrified in an IA or HDA state. This is because the density of water in these states is larger than the density of ice Ih and Ic. Hence, upon isochoric heating, the density of these amorphous ices would be incompatible to the rather low density of ice Ih and Ic. From the molecular point of view, IA and HDA contain molecules with $n \geq 5$ nearest neighbors. As such, these molecules have distorted tetrahedral environments that are not compatible to ice Ih and Ic. Therefore, it is suggestive to think of such highly-coordinated, HDA-like, molecules as 'ice suppressant'. Accordingly, such HDA-like molecules may provide a cryoprotectant environment to biomolecules, without the need to use undesired cryoprotectants and additives, such as sugars and alcohols.[35] An interesting question that deserves further study is how the presence of co-solutes and changes in pH may affect our results and, more generally, the cryopreservation of biomolecules. Confirmation of these ideas requires, of course, additional experiments.

5 Conflicts of interest

There are no conflicts to declare.

Acknowledgments

This work was supported by the SCORE Program of the National Institutes of Health under award number 1SC3GM139673. We thank the NSF CREST Center for Interface Design and Engineered Assembly of Low Dimensional systems (IDEALS), NSF grant number HRD-1547830, for additional support. This work was also supported, in part, by a grant of computer time from the City University of New York High Performance Computing Center under NSF Grants CNS-0855217, CNS-0958379 and ALI-1126113.

References

(1) L. Parmegiani, C. Garello, F. Granella, D. Guidetti, S. Bernardi, G. E. Cognigni, A. Revelli and R. Filicari, *Reprod. BioMed. Online*, 2009, **19**, 374-379.

(2) K. L. Scott, J. Lecak and J. P. Acker, *Transfus. Med. Rev.*, 2005, **19**, 127-142.

(3) R. J. de Vries, S. N. Tessier, P. D. Banik, S. Nagpal, S. E. J. Cronin, S. Ozer, E. O. A. Hafiz, T. M. van Gulik, M. L. Yarmush, J. F. Markmann, M. Toner, H. Yeh and K. Uygun, *Nature Biotechnology*, 2019, **37**, 1131-1136.

(4) F. Franks, *Biophy. Chem.*, 2003, **105**, 251-261.

(5) M. Adrian, J. Dubochet, J. Lepault and A. W. McDowall, *Nature*, 1984, **308**, 32-36.

(6) K. M. Yip, N. Fischer, E. Paknia, A. Chari and H. Stark, *Nature*, 2020, **587**, 157-161.

(7) T. Nakane, A. Kotecha, A. Sente, G. McMullan, S. Masiulis, P. M. Brown, I. T. Grigoras, L. Malinauskaite, T. Malinauskas, J. Miehling and T. Uchaski, *Nature*, 2020, **587**, 152-156.

(8) D. Cressey and E. Callaway, *Nature*, 2017, **550**, 167.

(9) C. U. Kim, J. L. Wierman, R. Gillilan, E. Limac and S. M. Gruner, *J. Appl. Cryst.*, 2013, **46**, 234-241.

(10) D. Quirnheim Pais, B. Rathmann, J. Koepke, C. Tomova, P. Wurzinger and Y. A. Thielmann, *Acta Cryst.*, 2017, **D73**, 997-1006.

(11) J. W. Pflugrath, *Acta Crystallogr. F Struct. Biol. Commun.*, 2015, **71**, 622-642.

(12) P. Ball, *Proc. Natl. Acad. Sci. U.S.A.*, 2017, **114**, 13327-1335.

(13) F. Franks, *Water: A Matrix of Life*, Royal Society of Chemistry, 2007.

(14) P. G. Debenedetti, *Metastable Liquids: Concepts and Principles*, Princeton University Press, 1996, vol. 1.

(15) N. Shimizu, K. Hirata, K. Hasegawa, G. Ueno and M. Yamamoto, *J. Synchrotron Radiat.*, 2007, **14**, 4-10.

(16) E. F. Garman and T. R. Schneider, *J. Appl. Cryst.*, 1997, **30**, 211-237.

(17) I. Hurbain and M. Sachse, *Biol. Cell*, 2011, **103**, 405-420.

(18) J. Dubochet, M. Adrian, J. J. Chang, J. C. Homo, J. Lepault, A. W. McDowall and P. Schultz, *Rev. Biophys.*, 1988, **21**, 129-228.

(19) K. B. Storey and J. M. Storey, *Scientific American*, 1990, **263**, 92-97.

(20) H. T. Merymar, *Annu. Rev. Biophys. Bioeng.*, 1974, **3**, 341-363.

(21) P. Mazur, *Science*, 1970, **168**, 939-949.

(22) K. C. Fox, *Science*, 1995, **267**, 1922-1923.

(23) A. Arsiccio, J. McCarty, R. Pisano and J. E. Shea, *J. Am. Chem. Soc.*, 2020, **142**, 5722-5730.

(24) K. L. McDonald, *Methods Cell Biol.*, 2007, **79**, 23-56.

(25) P. Echlin, *Plenum Press*, **1992**.

(26) J. Dubochet and A. W. McDowall, *J. Microscopy*, 1981, **124**, RP3-RP4.

(27) P. Bruggeller and E. Mayer, *Nature*, 1980, **288(5791)**, 569-571.

(28) S. De Carlo, *Plunge freezing (Holey Carbon Method). In Handbook of Cryo-preparation Methods for Electron Microscopy* (Cavelier, A., Spehner, D. and Humbel, B.M., eds), CRC Press, Boca Raton, FL, 2009 pp 49-68.

(29) J. Escaig, *J. Microsc.*, 1982, **126**, 221-229.

(30) U. Riehle and M. Hoechli, *Freeze-Etching Technique and Applications. Societe Francaise de microscopie Electronique, Paris*, 1973, 31-60.

(31) C. Hoffmann, A. Leis, M. Niederweis, J. M. Plitzko and H. Engelhardt, *Proc. Natl. Acad. Sci. U.S.A.*, 2008, **105**, 3963-3967.

(32) A. Al-Amoudi, J. J. Chang, A. Leforestier, A. McDowall, L. M. Salamin, L. P. O. Norlen, K. Richter, B. N. Sartori, D. Studer and J. Dubochet, *EMBO J.*, 2004, **23**, 3583-3588.

(33) K. L. McDonald, *J. Microsc.*, 2009, **235**, 273-281.

(34) R. Dahl and L. A. Staehelin, *J Electron. Microsc. Tech.*, 1989, **13**, 165-174.

(35) C. U. Kim, R. Kapfer and S. M. Gruner, *Acta Cryst.*, 2005, **D61**, 881-890.

(36) U. F. Thomanek, F. Parak, R. L. Mo ssbauer, H. Formanek, P. Schwager and W. Hoppe, *Acta Cryst.*, 1973, **A29**, 263-265.

(37) P. Urayama, N. P. George and S. M. Gruner, *Structure*, 2002, **10**, 51-60.

(38) C. Mueller-Dieckmann, B. Kauffmann and M. S. Weiss, *J. Appl. Cryst.*, 2011, **44**, 433-436.

(39) P. G. Debenedetti, *J. Phys.: Condens. Matter*, 2003, **15**, R1669-R1726.

(40) T. Loerting and N. Giovambattista, *J. Phys.: Condens. Matter*, 2006, **18**, R919-R977.

(41) P. H. Handle, T. Loerting, and F. Sciortino, *Proc. Natl. Acad. Sci. USA*, 2017, **114**, 13336-13344.

(42) O. Mishima and H. E. Stanley, *Nature*, 1998, **396**, 329-335.

(43) O. Mishima, *J. Chem. Phys.*, 1994, **100**, 5910-5912.

(44) K. Winkel, E. Mayer and T. Loerting, *J. Phys. Chem. B*, 2011, **115**, 14141-14148.

(45) P. Gallo, K. Amann-Winkel, C. A. Angell, M. A. Anisimov, F. Caupin, C. Chakravarty, E. Lascaris, T. Loerting, A. Z. Panagiotopoulos, J. Russo, J. A. Sellberg, H. E. Stanley, H. Tanaka, C. Vega, L. Xu and L. G. Pettersson, *Chem Rev.*, 2016, **116**, 7463-7500.

(46) P. Brüggeller and E. Mayer, *Nature*, 1980, **288**, 569-571.

(47) O. Mishima, L. D. Calvert and E. Whalley, *Nature*, 1984, **310**, 393-395.

(48) O. Mishima, L. D. Calvert and E. Whalley, *Nature*, 1985, **314**, 76-78.

(49) O. Mishima and Y. Suzuki, *J. Chem. Phys.*, 2001, **115**, 4199-4202.

(50) C. U. Kim, Y. F. Chen, M. W. Tate and S. M. Gruner, *J. Appl. Cryst.*, 2008, **41**, 1-7.

(51) Y. Suzuki and O. Mishima, *J. Chem. Phys.*, 2014, **141**, 094505.

(52) K. H. Kim, K. Amann-Winkel, N. Giovambattista, A. Späh, F. Perakis, H. Pathak, M. Ladd Parada, C. Yang, D. Mariedahl, T. Eklund, T. J. Lane, S. You, S. Jeong, M. Weston, J. H. Lee, I. Eom, M. Kim, J. Park, S. H. Chun, P. H. Poole and A. Nilsson, *Science*, 2020, **370**, 978-982.

(53) J. Huang and A. D. MacKerell Jr., *J. Comp. Chem.*, 2013, **34**, 2135-2145.

(54) J. L. F. Abascal and C. A. Vega, *J. Chem. Phys.*, 2005, **123**, 234505.

(55) J. Engstler and N. Giovambattista, *J. Chem. Phys.*, 2017, **147**, 074505.

(56) J. Wong, D. A. Jahn and N. Giovambattista, *J. Chem. Phys.*, 2015, **143**, 074510.

(57) P. H. Handle, F. Sciortino and N. Giovambattista, *J. Chem. Phys.*, 2019, **150**, 244506.

(58) F. Martelli, N. Giovambattista, S. Torquato and R. Car, *Phys. Rev. Materials*, 2018, **2**, 075601.

(59) M.J. Abraham, D. van der Spoel, E. Lindahl, B. Hess, and the GROMACS development team, GROMACS User Manual version 5.1.4, www.gromacs.org (2016).

(60) The Ow-Ow RDFs are calculated over all molecules of the system and without taking into consideration the volume excluded by the presence of polyalanine. We confirm that the RDFs are unchanged if we calculate the Ow-Ow RDF within a smaller volume in the system that excludes polyalanine. This is because our system contains a large number of water molecules ($N = 6857$) and only one polyalanine peptide.

(61) P. G. Debenedetti, F. Sciortino and G. H. Zerze, *Science*, 2020, **369**, 289-292.

(62) T. E. Gartner III, S. Torquato, R. Car and P. G. Debenedetti, *Nat. Comm.*, 2021, **12**, 3398.

(63) K. Amann-Winkel, D. T. Bowron and T. Loerting, *Molecular Physics*, 2019, **117**, 3207-3216.

(64) A. B. Almeida, S. V. Buldyrev, A. M. Alencar and N. Giovambattista, *J. Phys. Chem. C*, 2021, **125**, 5335-5348.

(65) J. Chiu, F. W. Starr and N. Giovambattista, N. *J. Chem. Phys.*, 2013, **140**, 114504.

(66) K. Heremans, *Ann. Rev. Biophys. Bioeng.*, 1982, **11**, 1-21.

(67) J. Bachler, P. H. Handle, N. Giovambattista and T. Loerting, *Phys. Chem. Chem. Phys.*, 2019, **21**, 23238-23268.

Table 1: Average properties of polyalanine in the different states A, A', B, B', B", X, and Y indicated in Fig. 1(b)-(c). R_g and L_p are, respectively, the peptide radius of gyration R_g and length. n_{HB} is the number of internal hydrogen-bonds of polyalanine and $d_{C\alpha C\alpha}$ is the average distance between nearest-neighbor C_α carbons. SASA is the solvent accessible surface area. Number in parenthesis are the standard deviations.

State	R_g [nm]	n_{HB}	L_p [nm]	$d_{C_\alpha C_\alpha}$ [nm]	SASA [nm^2]
A	0.932 (0.007)	16.895 (0.552)	3.232 (0.041)	0.3830 (0.0001)	16.110 (0.294)
A'	0.925 (0.001)	17.122 (0.081)	3.193 (0.012)	0.3830 (0.0001)	15.953 (0.038)
B	0.925 (0.005)	17.768 (0.399)	3.208 (0.034)	0.3840 (0.0002)	15.766 (0.220)
B'	0.919 (0.003)	17.552 (0.555)	3.142 (0.084)	0.3830 (0.0002)	15.787 (0.121)
B"	0.924 (0.003)	17.554 (0.559)	3.158 (0.084)	0.3840 (0.0002)	15.832 (0.157)
X	0.899 (0.004)	17.864 (0.130)	3.103 (0.023)	0.3820 (0.0002)	15.521 (0.246)
Y	0.925 (0.008)	17.885 (0.197)	3.202 (0.035)	0.3830 (0.0002)	15.822 (0.283)

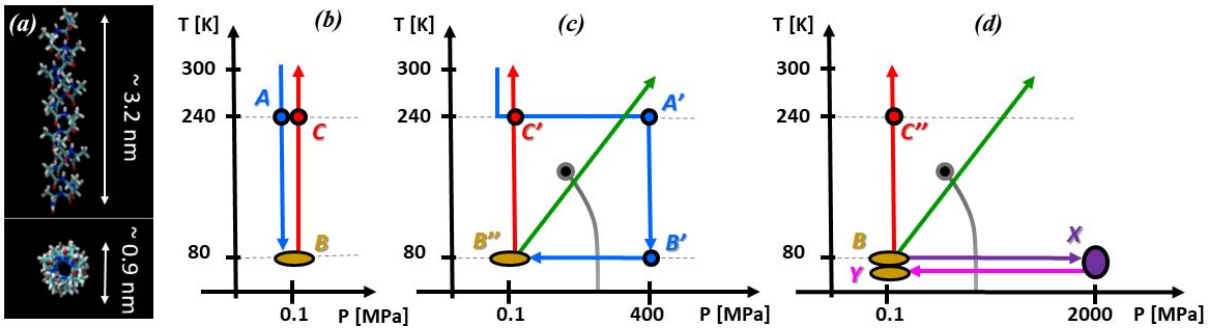

Figure 1: (a) Snapshots of the polyalanine peptide used in this work. The peptide is composed of 20 alanine amino acids which arrange in an alpha-helix configuration at normal conditions. (b)(c)(d) Thermodynamic paths studied in this work. (b) Hyperquenching of the system at $P = 0.1$ MPa (blue arrow) from the equilibrium liquid state (A) down to cryogenic temperatures (B), at which water is in the LDA state. Recovery of the sample is induced by isobaric heating (red arrow, $P = 0.1$ MPa). (c) High-pressure cooling of the system (blue arrow). The system is equilibrated at $T = 240$ K and $P = 0.1$ MPa (LDL-like water) followed by isothermal compression to $P = 400$ MPa (A'), at which water is in an HDL-like state. The system is then hyperquenched isobarically to cryogenic temperatures (B') at which water is in an amorphous ice state. The sample is then decompressed at $T = 80$ K to $P = 0.1$ MPa (state B") where water remains in a somewhat dense amorphous ice state. Recovery is performed by isobaric heating at $P = 0.1$ MPa (red arrow) and isochoric heating at $\rho \approx 1.15$ g/cm^3 (green arrow). (d) The polyalanine-water system produced in state B [see (b)], at which water is in the LDA state, is compressed at $T = 80$ K up to $P = 2000$ MPa, where water forms HDA (state X); the obtained polyalanine-HDA system is then decompressed back to $P = 0.1$ MPa (state Y). In (c) and (d), the LLCP and first-order LLPT line of *bulk* water are included (gray circle and line); the paths shown in (b) occur below the LLCP pressure (of *bulk* water). The cooling/heating rate is $q_T = 1$ K/ns; the compression/decompression rate is $q_P = 10$ MPa/ns.

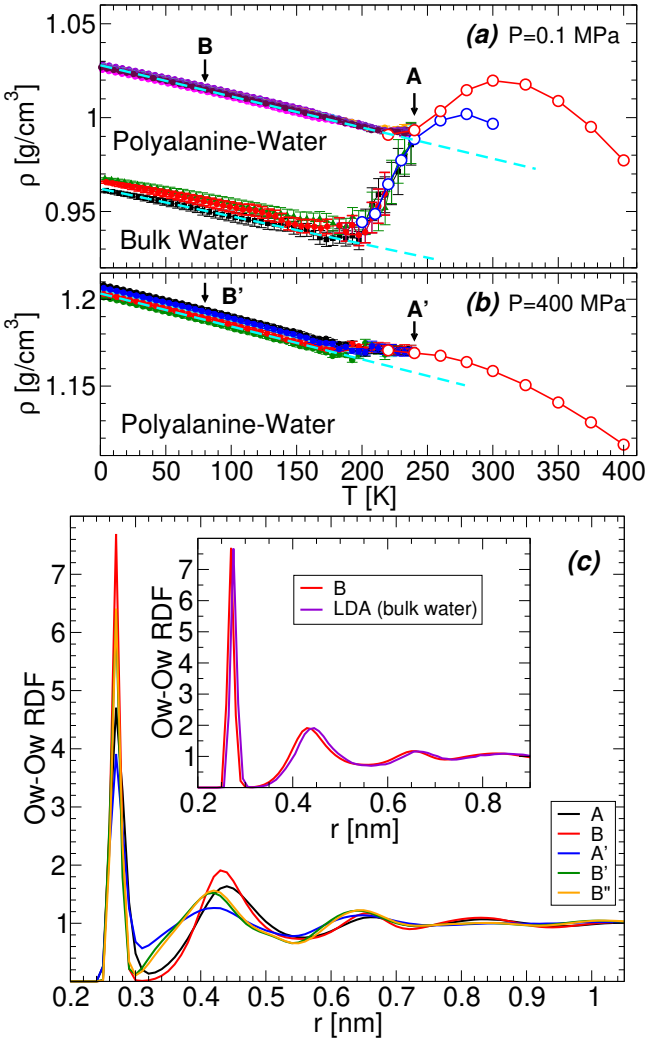

Figure 2: Density as function of temperature of the polyalanine-water system during cooling at (a) $P = 0.1$ MPa and (b) 400 MPa; the cooling rate is $q_T = 1$ K/ns. For comparison, also included in (a) is the $\rho(T)$ of bulk water cooled at $P = 0.1$ MPa [$q_T = 1$ K/ns, black and green symbols; $q_T = 0.1$ K/ns, red symbols] (from Ref.[56]). Equilibrium liquid densities are indicated by open circles. Results are for five independent trajectories of the polyalanine-water system, and two (one) independent runs for bulk water cooled at $q_T = 1$ K/ns ($q_T = 0.1$ K/ns). (c) Water Ow-Ow radial distribution function at the states A, B, A', B', B" indicated in Fig. 1. Inset: Comparison of the Ow-Ow RDF in state B and in *bulk* LDA (from Ref.[56]). The bulk LDA was produced by isobaric cooling of liquid water at $P = 0.1$ MPa and $q_T = 1$ K/ns.

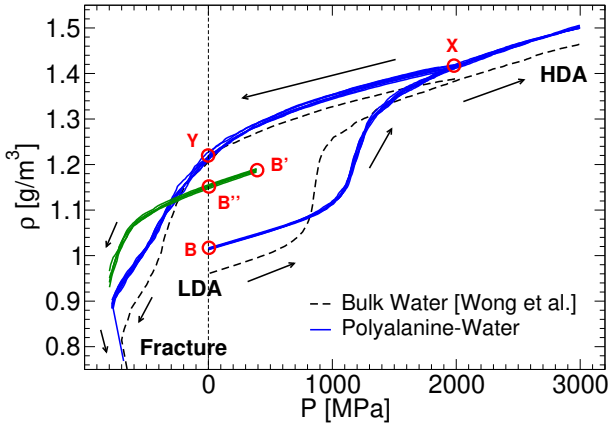

Figure 3: Density as function of pressure during compression and decompression of the polyalanine-water system along different thermodynamic paths; $T = 80$ K. Blue lines correspond to the compression/decompression-induced process shown in Fig. 1(d). Green lines correspond to the decompression of the system prepared by HPC at $P = 400$ MPa and $T = 80$ K [from state B' to state B"; see Fig. 1(c)]. All decompression paths are extended to negative pressures until the corresponding glass fractures. Dashed-lines are taken from Ref.[56] and correspond to the compression/decompression-induced LDA-HDA transformations in *bulk* TIP4P/2005 water. The compression/decompression rate is $q_P = 10$ MPa/ns in all cases.

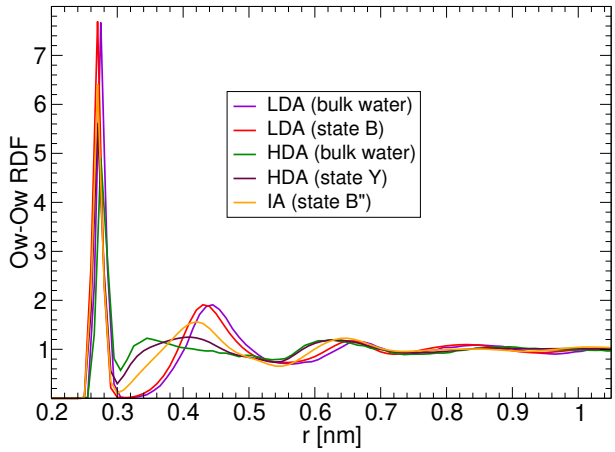

Figure 4: Water Ow-Ow RDF of the polyalanine-water system at $T = 80$ K and $P = 0.1$ MPa. RDFs are calculated for the system in states B, where water is in the LDA state, as well as B" and Y, where water is in an IA and HDA state, respectively. For comparison, we also include the RDF of *bulk* LDA and HDA (HDA is obtained by compression of LDA at $T = 80$ K to $P = 2000$ MPa, followed by decompression back to $P = 0.1$ MPa). The interstitial space at $r \approx 0.35$ nm is practically empty in the LDA samples; it is increasingly populated in the amorphous ices along the sequence of states B" $\rightarrow$ Y $\rightarrow$ bulk HDA.

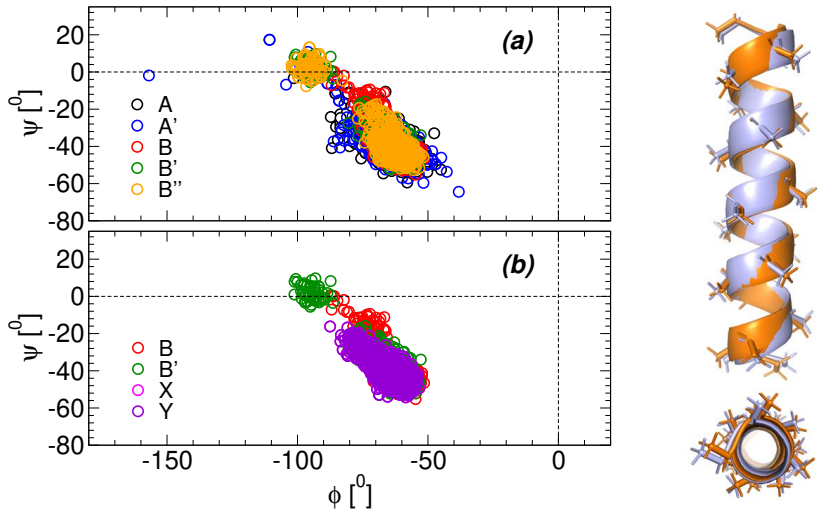

Figure 5: (a) Ramachandran plots of polyalanine in states A, A', B, B', B", X, and Y; see Fig. 1(b)(c). (b) Ramachandran plots of polyalanine at selected states sampled during the compression/decompression cycle shown in Fig. 3 (blue lines). The dihedral angles for an alpha helix peptide are approximately $-60^0 < \psi < 0^0$ and $-180^0 < \phi < -30^0$ and hence, polyalanine remains in its alpha helix configuration in all the states studied and independently of whether water is in the low- and high-density liquid states, IA, LDA, and HDA. The right panel shows superimposed snapshots of polyalanine in states B (orange) and B" (light blue). Similar snapshots are obtained when comparing polyalanine in other states (see SM).

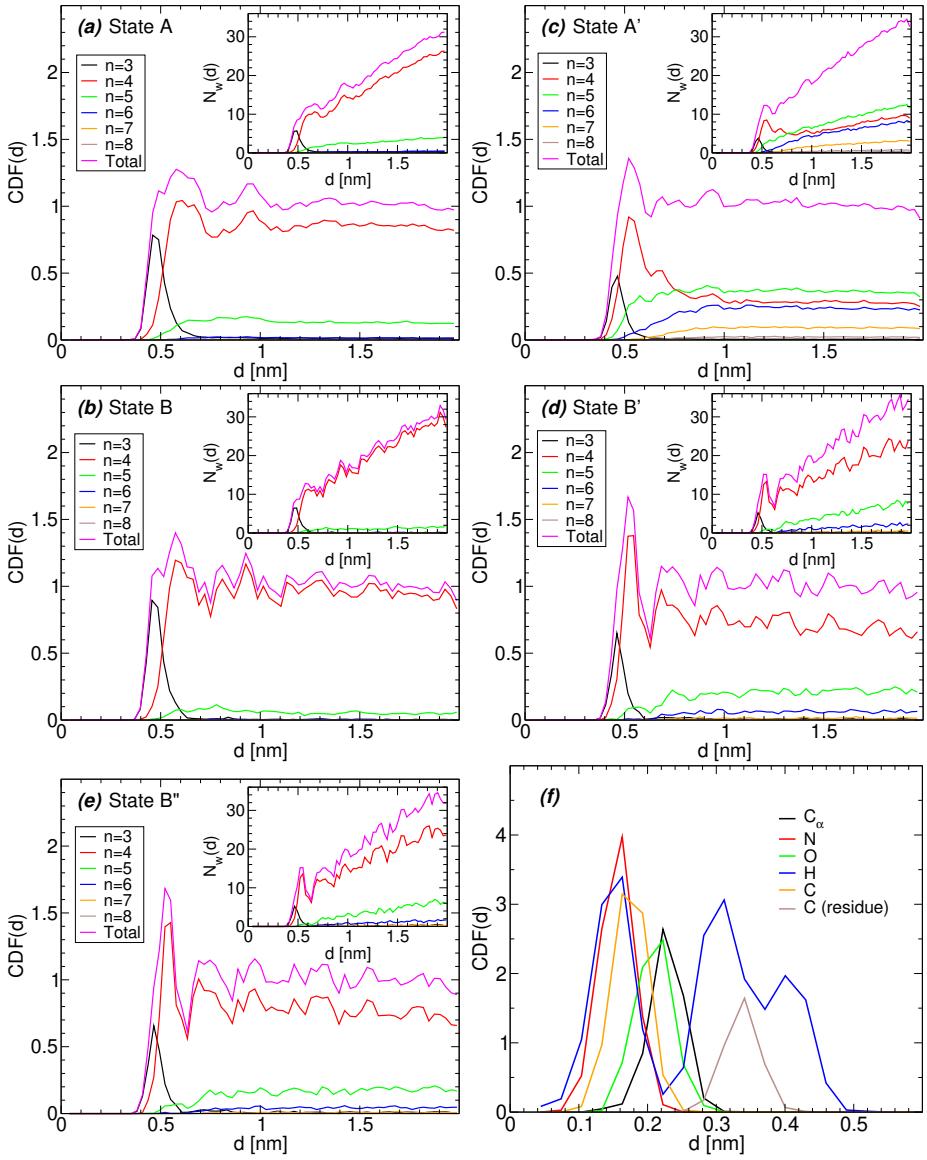

Figure 6: Cylindrical distribution functions of water at states (a) A (LDL-like), (b) B (LDA), (c) A' (HDL-like), (d) B' (IA, $P = 400$ MPa), and (e) B" (IA, $P = 0.1$ MPa) defined in Fig. 1(b)-(c). Included are the CDF for all molecules around polyalanine (magenta) as well as for molecules with $n = 3$ (black), 4 (red), 5 (green), 6 (blue), 7 (orange), and 8 (brown) nearest-neigbors. Insets in (a)-(e) are the corresponding number of molecules at a distance d from the peptide axis. (f) CDF of polyalanine atoms. The alanine side chains are located at the outer interface of polyalanine, at $d \approx 0.28 - 0.50$ nm; the atoms belonging to the peptide backbone are located in the inner regions of polyalanine. In the IA and LDA states, water molecules are surrounded mostly by 4 molecules; interfacial molecules with $n \geq 5$ are present only in the HDL-like state A'. The IA is composed mostly of molecules with $n = 4$ indicating that this is not a fully-developed HDA. Two molecules are considered neighbors if their Ow-Ow distance is less than $r_c \leq 0.34$ nm.

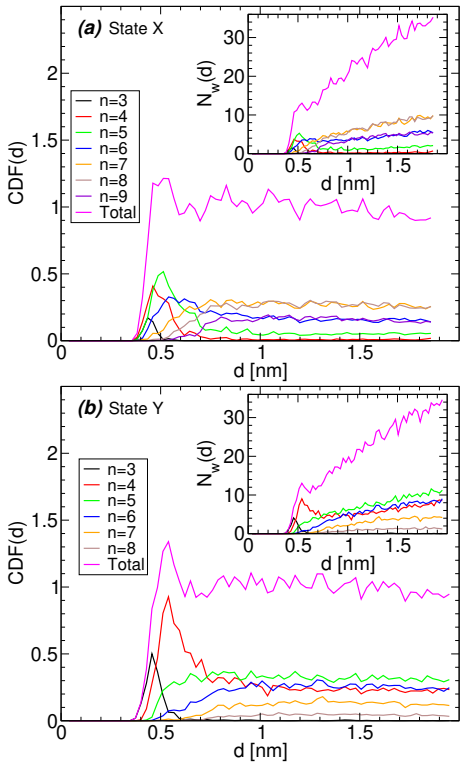

Figure 7: Cylindrical distribution functions of water around polyalanine at states (a) X and (b) Y sampled during the compression/decompression cycle at $T = 80$ K [see Fig. 3].

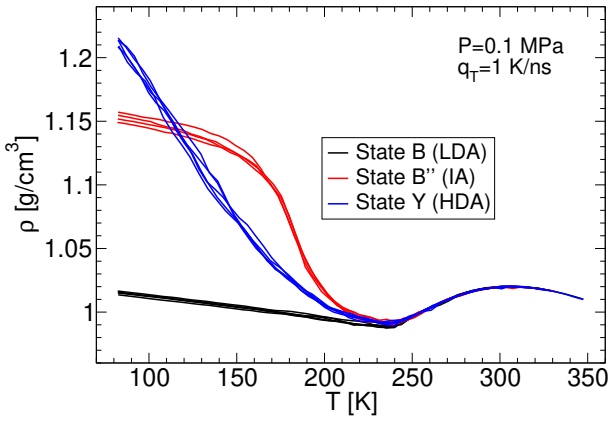

Figure 8: Density as function of temperature of the polyalanine-water system during isobaric heating at $P = 0.1$ MPa ($q_T = 1$ K/ns). The starting state of the system at $T = 80$ K are B (black), B" (red), and Y (blue) where water is, respectively, in an LDA, IA, and HDA state.

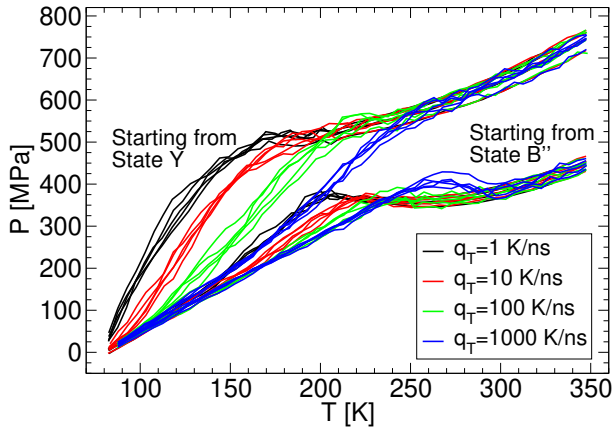

Figure 9: Pressure as function of temperature of the polyalanine-water system during heating at constant volume. Results are for the starting system being at state B" ($\rho = 1.15$ g/cm^3) and Y ($\rho = 1.21$ g/cm^3), where water is in an IA and HDA state, respectively. Black, red, blue, and green lines correspond to isochoric heating runs with heating rates $q_T = 1,\ 10,\ 100,\ 1000$ K/ns, respectively.